The effect of long-range order on intermolecular interactions in organic semiconductors: zinc octaethyl porphyrin molecular thin film model systems.

Kumar, A.; Naumenko, D.; Rossi, G.; Magnano, E.; Nappini, S.; Bondino, F.; Segoloni, E.; Amidani, L.; D'Acapito, F.; Boscherini, F.; Barba, L.; Pace, E.; Benfatto, M.; Casassa, S.; Pedio, M.;

Originally published:

November 2019

Physical Chemistry Chemical Physics 21(2019)41, 22966-22975

DOI: https://doi.org/10.1039/c9cp00954j

PCCP

PAPER

The effect of long-range order on intermolecular interactions in organic semiconductors: zinc octaethyl porphyrin molecular thin film model systems†

Cite this: DOI: 10.1039/c9cp00954j

A. Kumar, ‡[ab] D. Naumenko,‡§[a] G. Rossi,[c] E. Magnano,[ad] S. Nappini,[a] F. Bondino,[a] E. Segoloni,[a] L. Amidani,¶[c] F. d'Acapito,[e] F. Boscherini,[c] L. Barba,[f] E. Pace,[g] M. Benfatto,[g] S. Casassa[h] and M. Pedio[a]

Received 17th February 2019,
Accepted 25th September 2019

DOI: 10.1039/c9cp00954j

rsc.li/pccp

In order to optimize the performance of devices based on porphyrin thin films it is of great importance to gain a physical understanding of the various factors which affect their charge transport and light-harvesting properties. In this work, we have employed a multi-technique approach to study vacuum deposited zinc octaethyl porphyrin (ZnOEP) thin films with different degrees of long-range order as model systems. An asymmetrical stretching of the skeletal carbon atoms of the porphyrin conformer has been observed and attributed to ordered molecular stacking and intermolecular interactions. For ordered films, a detailed fitting analysis of the X-ray absorption near edge structure (XANES) using the MXAN code establishes a symmetry reduction in the molecular conformer involving the skeletal carbon atoms of the porphyrin ring; this highlights the consequences of increased π–π stacking of ZnOEP molecules adopting the triclinic structure. The observed asymmetrical stretching of the π conjugation network of the porphyrin structure can have significant implications for charge transport and light harvesting, significantly influencing the performance of porphyrin based devices.

Introduction

Small conjugated organic molecules are promising candidates for novel optoelectronic devices due to their favorable optical and semiconducting properties.[1] Among conjugated organic molecules, thin films (TFs) based on tetrapyrrole complexes have been utilized in optoelectronic devices as charge transport and injection layers.[2] These molecular TFs have shown promising applications in thin film organic field-effect transistors (OFETs), organic light emitting diodes (OLEDs) and organic photovoltaic devices.[3–5] Due to such important applications, considerable attention has been given to understand the various factors influencing charge carrier mobility and light harvesting ability of molecular TFs.

In contrast to inorganic semiconductors, charge transport in organic semiconductors exhibits a strong dependence on weak van der Waals interactions between adjacent molecules.[6] Intermolecular interactions depend on molecular stacking, polymorphism and crystallinity of TFs, which in turn depend on the synthesis procedure, nature of the substrate and post-growth treatment.[7] Therefore, many of the physical properties of the TFs are strongly influenced by these factors since they influence the degree of intermolecular orbital overlap.[8] Differences in molecular stacking, for example due to polymorphism and different degrees of long range order, lead to anisotropy in the charge transport and optical absorption properties of crystalline molecular films. The mobility is also dependent on the packing of the organic molecules in the film and it is found to be higher when the direction of π-overlap coincides with the direction of current flow. It has been observed that crystalline tetrapyrrole complex TFs with face-on orientation exhibit

[a] Istituto Officina dei Materiali, Consiglio Nazionale delle Ricerche, TASC Laboratory, Trieste, Italy
[b] Dipartimento di Fisica, Università di Trieste, Trieste I-34127, Italy
[c] Department of Physics and Astronomy, University of Bologna, Italy
[d] Department of Physics, University of Johannesburg, PO Box 524, Auckland Park, 2006 Johannesburg, South Africa
[e] Istituto Officina dei Materiali, Consiglio Nazionale delle Ricerche, c/o ESRF, Grenoble, France
[f] Istituto CNR-IC, Area Science Park Basovizza, Trieste, 34149, Italy
[g] LNF-INFN, Frascati 00044, Italy
[h] Dipartimento di Chimica, Università di Torino and NIS, Nanostructured Interfaces and Surfaces, Centre of Excellence, Via Giuria 5, 10125 Torino, Italy

† Electronic supplementary information (ESI) available. See DOI: 10.1039/c9cp00954j

‡ These authors contributed equally to this work.
§ Present address: Elettra Sincrotrone Trieste, Area Science Park Basovizza, Trieste 34149, Italy.
¶ Present address: ROBL beamline at ESRF, Grenoble, France.

higher optical absorption than in the case of edge-on orientation; moreover, the power conversion efficiency for the face-on configuration is almost double that for edge-on orientation.[3] In addition, the mobility of organic semiconductors has been found to increase with temperature due to an improved morphological homogeneity of the film.[6] The diffusion length of excitons and charge carrier mobilities are found to be larger in crystalline films than in their amorphous counterparts,[11,12] while quantum-chemical calculations confirm that the molecular packing and density of chemical and/or structural defects significantly influence charge transport in organic semiconductors.[13]

The photovoltaic conversion efficiency has been found to be related to the degree of long-range order in ZnOEP films.[9] In the case of C_{60}-ZnOEP heterojunctions the hole mobility in the ZnOEP films becomes higher upon crystallization,[10] which increases the number of inter-molecular charge-transfer excitons and enhances charge carrier mobility. It also results in a significant improvement of photoabsorption efficiency under illumination. Furthermore, the charge carrier mobility in field-effect transistors based on metal octaethyl porphyrins in the triclinic (TR) phase with various central metal atoms has been found to increase with decreasing intermolecular distance.[14] Field effect mobility has been found to be dependent on molecular orientation: vertically aligned Platinum OctaEthyl Porphyrin (PtOEP) molecules (edge-on) show 100 times higher field effect mobility as compared to horizontally aligned (flat-on) PtOEP ones.[15]

In addition to charge carrier mobility, the light harvesting efficiency of porphyrin TFs is also influenced by the molecular packing and long range order. Theoretical calculations show that the optical properties of porphyrin molecules are strongly dependent on the π conjugation network.[16]

In order to illustrate the dependence of optical properties on ordering, in Fig. 1(a) we report the optical absorption spectra of differently ordered ZnOEP films on a transparent indium tin oxide (ITO) substrate, the gas phase molecules and the molecules in solution; it can be noticed that the ratio between the intensity of the Q band and that of the Soret band is higher for semiordered ZnOEP films compared to a disordered film. Furthermore, the optical absorption spectra obtained in solution[17] and the gas phase[18] are significantly different from those of ZnOEP films, highlighting the impact of molecular packing and long range order.

Moreover, it has been observed that the proximity of ethyl groups in the triclinic structure of ZnOEP influences their vibrational properties. In fact, a combined infrared vibrational spectroscopy and X-ray diffraction study of ZnOEP TFs on quartz substrates revealed that the asymmetric vibration of CH_3 units is hindered due to the proximity with the CH_2 groups of the neighboring ZnOEP molecule and results in the suppression of the IR peak due to asymmetric vibration of CH_3 (1446 cm^{-1}).[19] This peak is restored for amorphous ZnOEP/C_{60} films highlighting the impact of intermolecular interactions on the properties of ZnOEP TFs.

Due to the favorable optical absorption properties of ZnOEP in the visible region and implications for applications in

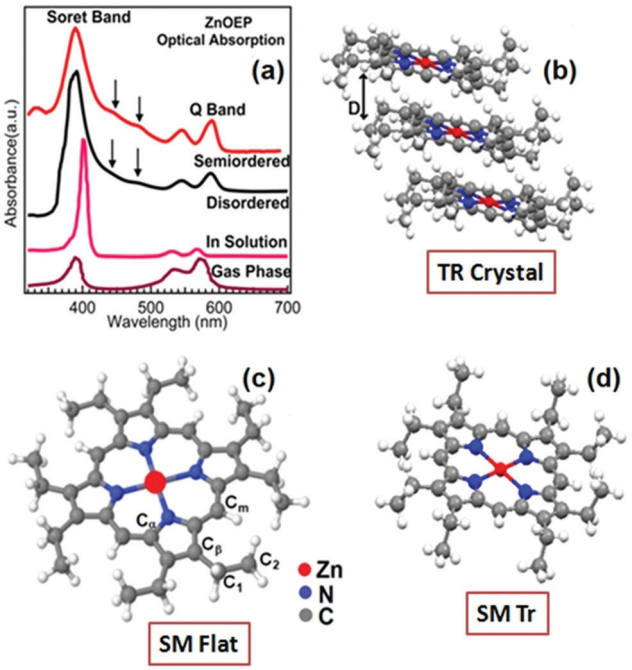

Fig. 1 (a) Optical absorption spectra of disordered and semiordered ZnOEP thin films on ITO are compared to the literature spectra in the gas phase and ZnOEP dissolved in dichloromethane. Peaks labeled with arrows are related to the inter-molecular charge-transfer excitons in the films.[7] (b) ZnOEP molecules in the triclinic crystal structure are labeled as TR crystals, *D* indicates the distance between adjacent molecular planes (~3.4 Å). The ZnOEP conformers: (c) single ZnOEP molecule with in-plane ethyl groups labelled as SM (single molecule) flat and (d) ZnOEP molecule with out-of-plane orientation of the ethyl groups (*trans* configuration) labelled as SM Tr.

functional molecular devices, we devote the present study to highlighting the impact of the molecular packing and long range order of the π conjugation network. Generally, porphyrins present a pronounced tendency for polymorphism in crystal packing. Instead, ZnOEP is considered a good model system,[20] which has no structural polymorphism as a triclinic single crystal.[21,22]

The ZnOEP molecule can adopt two conformers that differ in mutual orientations of the ethyl groups. As shown in Fig. 1 the ZnOEP molecule with in-plane ethyl groups is labelled as SM (single molecule) flat (gas phase and solutions). In the solid triclinic structure, labelled SM Tr, the ethyl-groups are in a *trans* configuration with respect to the basal plane with four ethyl groups pointing upwards and the other four pointing downwards, probably to reduce steric (and repulsion) effects.

In this work we adopt a multi-technique characterization approach to study ZnOEP TFs using Raman spectroscopy, grazing incidence X-ray diffraction (GIXRD), atomic force microscopy (AFM) and X-ray absorption fine structure (XAFS) analysis.

Our results indicate that the degree of order in the ZnOEP TFs is determined by the substrate, its treatment and by the growth procedures. We found that higher molecular order leads to greater overlap of π–π orbitals and results in the symmetry

reduction of ZnOEP conformers involving the skeletal carbon atoms.

Experimental methods

The bulk sample was a commercial high purity ZnOEP polycrystalline powder (Sigma Aldrich). ZnOEP TFs, thickness ~40 nm, were deposited *ex situ* by sublimation under UHV, at a deposition rate of ~2 Å min^{-1} (base pressure 2×10^{-10} mbar, pressure during deposition 5×10^{-9} mbar) from resistively heated quartz crucibles containing ZnOEP powders. The thickness was measured using an oscillating quartz microbalance. The ZnOEP molecules were deposited at room temperature (RT) on silicon wafers and ITO substrates, with a roughness of 0.2 nm and 1.7 nm, respectively. The ITO substrates were rinsed with acetone before introducing them in the UHV chamber. The silicon substrates (un-doped) with 40 Å of native oxide (SILTRONIX) were used either without further treatment or annealed at 300 °C under UHV. In order to increase the ordering, the annealing of the TFs was performed after deposition at 80 °C, a temperature far below the sublimation point (about 270 °C) for 10 hours under UHV. All the measurements on *ex situ* samples were performed on freshly prepared TFs. Extended X-ray Absorption Fine Structure (EXAFS) and Near Edge X-ray Fine Spectroscopy (NEXAFS) or X-ray Absorption Near Edge Structure XANES[23] measurements at the Zn K edge were performed at the ''GILDA/LISA'' BM-08 beamline[24] of the European Synchrotron Radiation Facility (ESRF, Grenoble France). The films were measured in the fluorescence mode using a dynamically sagittally focusing Si(311) monochromator,[47] a hyper pure Ge detector and associated digital electronics with a 1 μs peaking time.[25] Higher order harmonics were eliminated with a pair of Pd coated grazing incidence mirrors. The energy spacing for the EXAFS spectra was equivalent to less than 0.05 $Å^{-1}$.

N K-edge NEXAFS spectroscopy and X-ray photoelectron spectroscopy (PES) measurements were carried out at the CNR beamline BACH, Elettra, at a base pressure $<10^{-9}$ mbar.[26] NEXAFS spectra were measured both in fluorescence yield (FY) using a multi channel plate (MCP) detector (F4655 Hamamatsu) and in total electron yield (TEY), ensuring either bulk or surface sensitivities, respectively. PES measurements were performed using a VG Scienta R3000 hemispherical electron analyzer.[27] A photon energy of 600 eV, corresponding to an inelastic mean free path in the range of 1 nm, was employed to compare the composition and contamination of *in situ* and *ex situ* samples.

The Zn K edge XANES spectra were simulated by means of the MXAN code,[28] by using the full multiple scattering (MS) approach within the muffin tin (MT) approximation and a complex potential. The real part of the exchange and correlation potential was calculated on the basis of the Hedin–Lundqvist approximation, and inelastic losses were taken into account. The zero-energy corresponds to the interstitial potential of the muffin-tin spheres. Muffin-tin radii and the interstitial potential were optimized during the fitting procedure.[29] The best fit condition was obtained by minimization of the R_{sq} function taken as the likelihood parameter as defined in ref. 28.

GIXRD measurements were performed at the X-ray diffraction beamline 5.2 at ELETTRA[30] following standard procedures.[31] Detailed information regarding GIXRD, AFM and Raman instrumentation along with a description of the approach adopted for simulating the Raman spectra are reported in the ESI.†

Results

In order to investigate the influence of substrates and growth procedures on the physical properties of the ZnOEP TFs, we investigated two types of samples: ZnOEP TFs grown on SiOx/Si or ITO at room temperature subjected to no further treatment and samples grown at RT and subsequently annealed. ZnOEP TFs deposited at RT on ITO and SiOx/Si are labeled as ''disordered/ITO'' and ''semiordered/Si'', respectively; annealed TFs on ITO and SiOx/Si are labeled as ''semiordered/ITO'' and ''ordered/Si'', respectively. This terminology will be explained in the next section.

Morphology and long range structural order

Fig. 2 shows the bidimensional diffraction patterns for the different classes of ZnOEP films, which clearly reflect differences in the long range order. Several diffraction spots are clearly detectable for the annealed ZnOEP TF on SiOx/Si demonstrating a highly crystalline and ordered structure. The diffraction spots are comparatively wider and relatively less intense at higher diffraction angles for the ZnOEP TF deposited at RT on SiOx/Si, therefore termed ''semiordered''. Annealing was also effective in obtaining a higher molecular order in TFs deposited on ITO. The rings in the bottom panels (c) and (d) are related to randomly oriented polycrystallites in the ITO substrate while Si bulk reflections are also visible in the upper panels.

GIXRD analysis shows that ZnOEP TFs adopt a triclinic structure with a = 4.692 Å, b = 13.185 Å, c = 13.287 Å, α = 113.94°, β = 91.177° and γ = 92.16°. The patterns are compatible with the reported triclinic structure[9,10,21] of the ZnOEP single crystal.[21] In all cases, including the disordered sample, the first order (higher intensity) reflections are detectable and exhibit good resemblance to the results obtained by laboratory sources.[45] The dominant orientation of crystallites for ordered, semiordered and disordered ZnOEP TFs is such that the [0 −1 1] direction is perpendicular to the substrate surface. No polymorphs were detected, while a certain degree of random misorientation of the crystallites was present, especially in annealed TFs on Si, giving rise to a faint powder-like component of the patterns.

The cell parameters were checked against reference data[21] by means of the Mercury[32] and SimDiffraction[33] codes, allowing indexing of all the reflections (see Fig. SI-1, ESI†). The positions and FWHM of peaks along the [0 −1 1] direction were extracted by means of Fit2d in association with WinPlotr.[34]

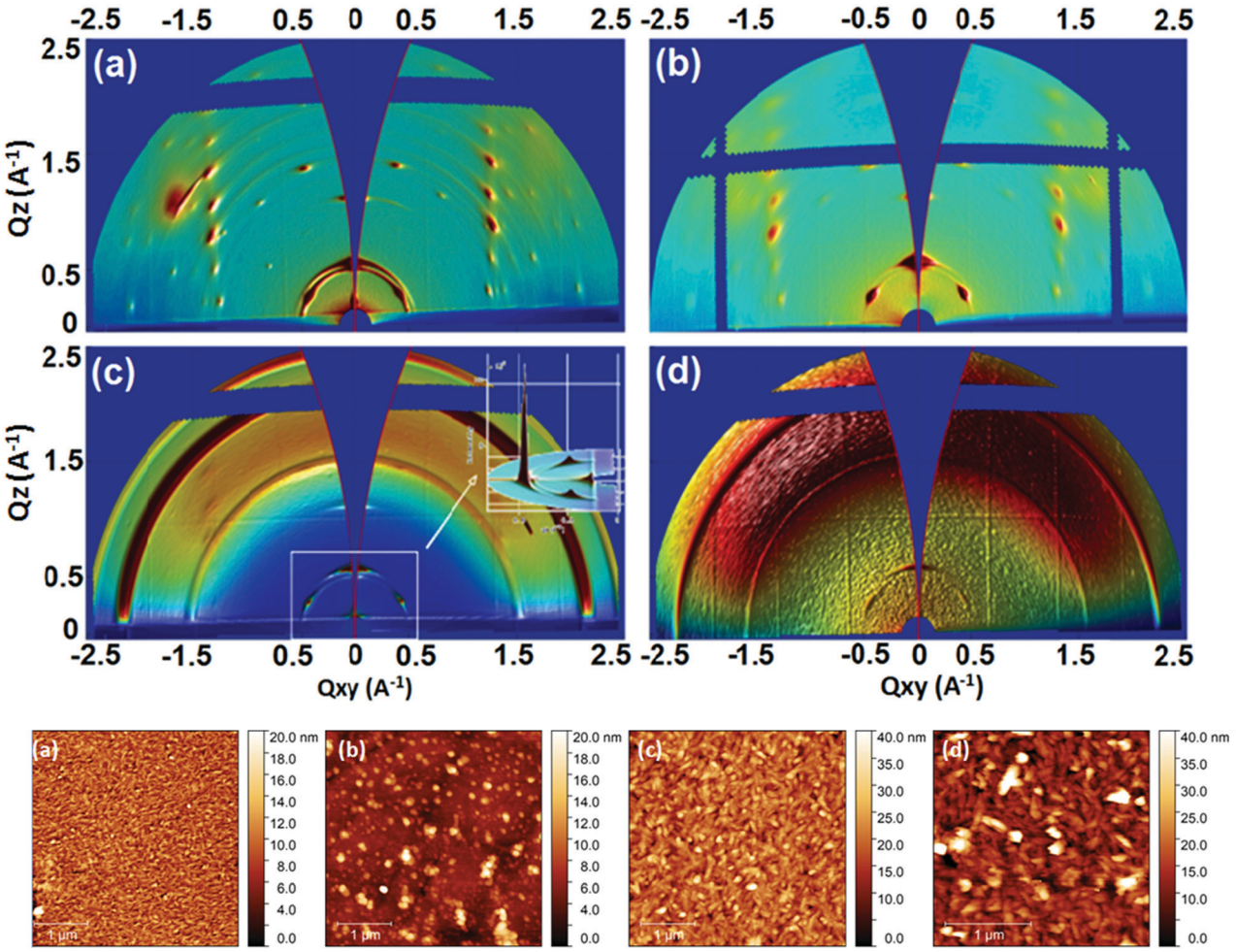

Fig. 2 Top panel: Bidimensional diffraction patterns at 0.04° incidence on the ZnOEP films (a) ordered/Si, (b) semiordered/Si, (c) semiordered/ITO and (d) disordered/ITO. The indexing has been assigned by means of the simulated XRD pattern (Fig SI-1, ESI†) from the literature reported structure.[21] Bottom panel: AFM images of ZnOEP films (a) ordered/Si, (b) semiordered/Si, (c) semiordered/ITO and (d) disordered/ITO.

Peak profile analysis has been performed by the WAXX code based on the Hosemann approach.[35] Furthermore, details are provided in the SI-1 section (ESI†).

The results are summarized in Table 1. Average sizes of crystallites were estimated and found to be lower for the films on the SiOx/Si substrate compared to ITO; this can be attributed to the different growth mechanisms induced by different surface and molecule–substrate interactions, indicating a higher disorder for depositions on ITO.

The average crystallite size and root mean square (rms) roughness determined from the analysis of AFM images (Fig. 2, bottom panel) are listed in Table 1 and show smaller grain size and lower surface roughness for the ordered film. In order to have quantitative characterization of the films, the power spectral density function, which provides a representation of the amplitude of the surface roughness as a function of the spatial frequency, was computed and is reported in Fig. SI-4 (ESI†). The evaluated crystallite size of the ordered ZnOEP TF is 20.2 nm while for the semiordered case (for both ITO and Si substrates) it is about 39.4 nm.

While the grain sizes measured by AFM and GIXRD have a similar dependence on the TF preparation, the values determined by AFM are in most case greater. This is because AFM provides information about agglomerated crystallites, *i.e.*

Table 1 Average grain sizes from AFM are compared to the crystallite size obtained from GIXRD peak profile analysis of the [0 −1 1] direction. See the ESI for details

Sample	GIXRD Average crystallite-volume-weighted size (nm)	AFM Average grain size (nm)	AFM rms roughness (nm)
Ordered/Si	22 ± 4	20 ± 5	2.25
Semiordered/Si	22 ± 1	39 ± 15	2.52
Semiordered/ITO	25 ± 1	39 ± 10	4.42
Disordered/ITO	29 ± 4	45 ± 15	7.39

domains of crystallites[36] while crystallite sizes determined by GIXRD are related to the coherent scattering domains in the specified crystallographic direction. Nevertheless, both GIXRD and AFM show that the crystallite size of ZnOEP TFs is the lowest for ordered films. A similar trend has been observed for phthalocyanine TFs.[37]

Vibrational properties

In order to investigate the implications of greater molecular order for the vibrational properties of ZnOEP TFs, Raman spectroscopy measurements and relative simulations have been performed; representative results are shown in Fig. 3. In the low frequency range the simulated Raman spectrum shows good agreement with the observed ordered film spectrum, as shown in Fig. 3a.

Ab initio calculations have been performed to simulate Raman spectra after the structural optimization of the ZnOEP molecule at the B3LYP-D* level. ZnOEP structural optimization confirms the *trans* configuration (Fig. 1). The detailed assignment of the peaks along with calculated Raman bands is reported in Table SI-5 (ESI†).[38,39] As shown in Fig. 3(a), the absence of a Raman shift for the vibrational modes involving the central metal atom bound to 4 N atoms in the macrocycle suggests that no significant structural changes occur in the macrocycle. Moreover, intermolecular interactions in the closely packed ordered films do not lead to macrocycle deformation. Instead, for skeletal carbon atom ($C_{\beta\beta}$, C_m, and C_α) vibrational modes, we observe small but notable Raman shifts indicating a probable structural deformation related to these atoms. Such Raman shifts, related to vibrational bands at 1561 cm^{-1} ($C_\beta C_\beta$), 1621 cm^{-1} ($C_\alpha C_m$) and 1376 cm^{-1} ($C_\alpha N$) due to π–π interactions, have been observed for CuOEP[40] and zinc(II) and palladium(II) octakis(β-decoxyethyl) porphyrins.[41] Notably, there is a significant decrease in the intensity of vibrational modes related to C–N–Zn (357 cm^{-1}) and Zn–N_4 (254 cm^{-1}) and 1561 cm^{-1} ($C_\beta C_\beta$), 1621 cm^{-1} ($C_\alpha C_m$) and 1376 cm^{-1} ($C_\alpha N$) for disordered film compared to ordered ones.

Due to different molecular stacking and higher disorder of ZnOEP molecules, the intensity of the Raman bands is least for disordered TFs deposited at RT on ITO. Such a sensitive dependence of macrocycle vibrational band intensities for the disordered film has been reported for titanylphthalocyanine TFs grown on amorphous quartz at different temperatures.[42] Disordered molecular stacking of phthalocyanine TFs deposited on ITO has been revealed by the dependence of macrocycle vibrational band intensity on molecular order.[37]

Two distinguishable peaks at 225 cm^{-1} and 245 cm^{-1} (calculated as 234 cm^{-1} and 249 cm^{-1}, respectively) are related to the vibrational modes of the ethyl groups.[39] In addition, modes at 1320 cm^{-1} and 1492 cm^{-1} are also related to peripheral ethyl group vibrations.[38,39] Calculations reveal that the anti-phase bending motions of the CH_3 and CH_2 moieties give rise to a set of peaks concentrated around 1500 cm^{-1} that is experimentally observed as a single peak at 1492 cm^{-1} only in the case of the ordered films deposited in SiOx/Si. As shown in Fig. 3(a) and (b) vibrational modes corresponding to external ethyl groups are much broader and exhibit lower intensity for the disordered film compared to the ordered one, further highlighting the influence of molecular order on vibrational properties. No significant differences are found in the Raman spectra of two semiordered samples (SiOx/Si and ITO). Moreover, a Bader analysis of the charge density reveals the formation of weak ionic-like inter-molecular interactions between protons belonging to the CH_3 moieties in different lattice planes. Such interactions are not expected for disordered films with randomly oriented ZnOEP molecules. This is compatible with intermolecular interactions being prevalent for ordered ZnOEP films and can have significant implications on the charge transport. Thus, differences in molecular packing lead to significant changes in intermolecular interactions, which are revealed by the Raman spectra. In order to establish structural deformations related to the C_β, C_m and C_α atoms for the as-deposited ZnOEP TFs a detailed structural analysis is needed to shed more light on this issue. We address this issue in the next section devoted to a thorough XAFS analysis.

Molecular orientation and short range order

XAFS measurements at the Zn K edge were performed in both the near edge and extended energy range on the different ZnOEP TF samples and a bulk polycrystalline ZnOEP one was

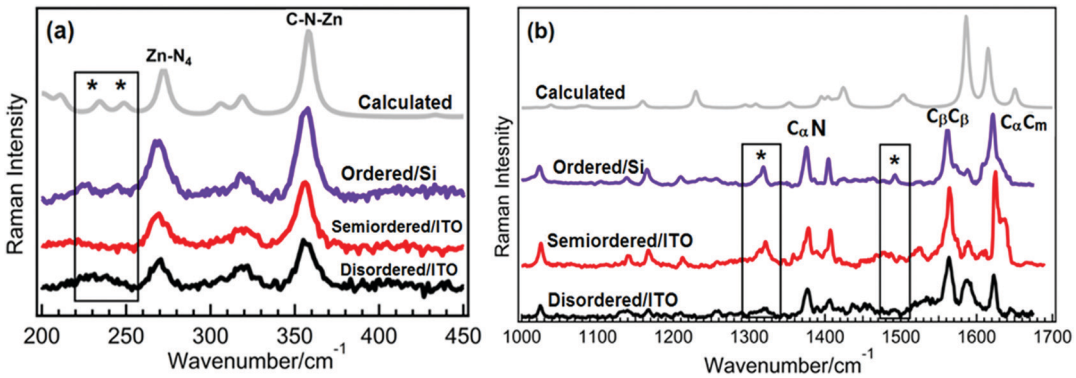

Fig. 3 Raman spectra of ZnOEP films acquired at 532 nm excitation wavelength in the ranges (a) 200–450 cm^{-1} and (b) 1000–1700 cm^{-1} compared to theoretical calculations of the frozen ZnOEP molecule. Peaks labelled as * are related to peripheral ethyl group vibrational modes.

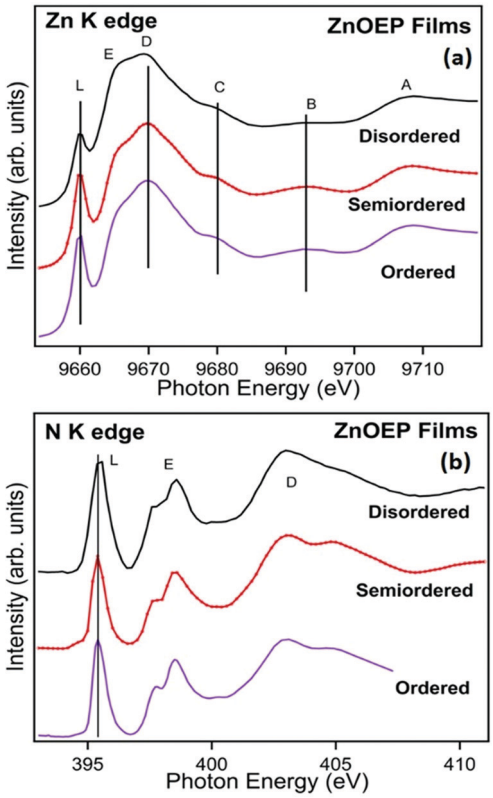

Fig. 4 (a) Normalized Zn K edge XANES and (b) N K edge XANES. Assignments of N K edge features are indicated, following ref. 10.

taken as a reference. Fig. 4(a) reports the Zn K edge XANES spectra normalized at 9720 eV taken with the sample plane at 55° with respect to the direction of the X-ray beam (the so-called "magic angle"). The feature labelled L around 9660 eV corresponds to the transition to the lowest unoccupied molecular orbital (LUMO) and in the case of the disordered film this peak shows a notable decrease in intensity with respect to the other cases. N K edge XAFS spectra (Fig. 4b) were taken on the same *ex situ* grown samples and in similarly *in situ* grown TFs. The spectral line shape is in agreement with the data reported in the literature.[43] A slight shift of the position of peak L and a general broadening is detected for disordered films compared to semiordered and ordered films. Even in this case, no significant differences were found in two semiordered samples (SiOx/Si and ITO).

In the case of the Zn K edge, based on our multiple scattering (MS) calculations (Fig. 7, right panel) we have assigned the sharp L peak as due purely to transitions to the π* LUMO, while the second feature labeled E is a combination of the upper orbitals LUMO+1 and LUMO+2.

The dependence of the intensity of peak L on the sample orientation, a linear dichroism effect, can measure the average tilt angle of ZnOEP molecules with respect to the growth plane; the procedure to determine the dichroic ratio R is described in Section S5 of the ESI.† The quantitative analysis takes into account the different degrees of X-ray polarization: 95% for the Zn K edge spectra and 100% for N K edge spectra.

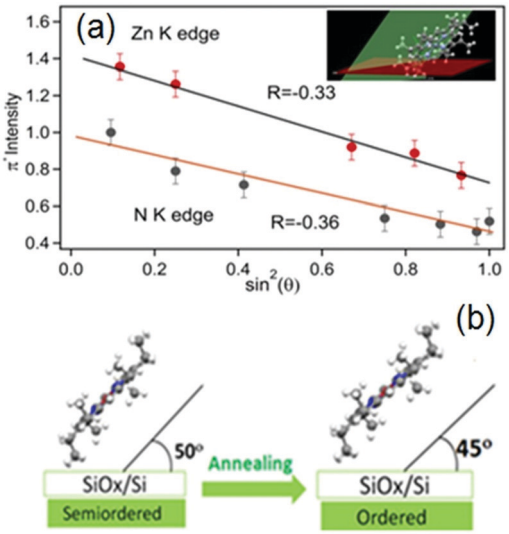

Fig. 5 (a) Analysis of the LUMO intensity *versus* angle of incidence for both edges. (b) Schematic representation of the ZnOEP molecular orientation for semiordered and ordered films based on XANES analysis.

As shown in Fig. 5(a) in the case of ordered ZnOEP TFs, we observe an R factor ranging between −0.33 and −0.36 (determined from the Zn and N edge data, respectively). If these films were completely crystalline, with a single crystal orientation, this tilt could be interpreted as a macrocycle plane tilt of ≈44° with respect to the substrate. For semiordered samples a similar analysis provides an average angle of about 50° (Fig. SI-7, ESI†). This value of the average tilt angle for the semiordered sample is in good agreement with the results discussed in ref. 45. Therefore, annealing of the semiordered sample leads to a change in the macrocycle plane tilt from 50° to 45° with respect to the substrate.

Finally, we note that the FY and TEY N K edge spectra of *in situ* and *ex situ* ZnOEP TFs did not show any difference (data not reported), indicating identical and uniform composition of the samples along the normal direction. No differences between *in situ* and freshly grown *ex situ* samples exposed to air and subsequent measured under UHV were observed. Only a weak oxygen contaminant was detected within the photoemission sensitivity in the freshly grown *ex situ* samples[46] limited to the first two layers of the films.

EXAFS analysis

Details on the EXAFS data reduction and analysis are given in the ESI,† SI-4. As for XANES, EXAFS spectra were measured at various orientations with respect to the linearly polarized X-ray beam, by varying the angle between the sample plane and the X-ray wave-vector (inset of Fig. 6), in order to probe linear dichroism effects. In Fig. 6 we report the continuous lines to be the magnitudes of the Fourier transforms, obtained in the range k = 2.8–7.5 Å^{-1}. A qualitative inspection indicates that the local structure of the films is rather similar to that of the bulk. However, the amplitude of the signals is significantly lower in the spectra of the annealed TF measured at θ = 20° and θ = 30°

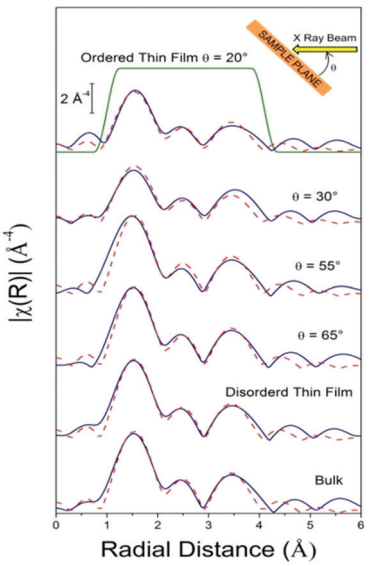

Fig. 6 Magnitude of the Fourier transforms of EXAFS signals weighted by k^3. The continuous blue lines are the experimental data while the dashed red lines are the fits obtained as described in the text.

relative to the others. As discussed in the section above and in the ESI,† the Zn K edge XANES spectra (Fig. SI-7) show a clear dependence linear dichroism, strongly suggesting that annealing induces an average orientational ordering of the molecular units composing the TF. Analysis of the EXAFS spectra was performed adopting a similar approach as in the case of transition metal phthalocyanines.[44] The fits of the data are reported as dashed lines in Fig. 6 and local structural parameters are listed in Table SI-7 (ESI†). The model structure is taken from ref. 21. The conclusion of the data analysis is that, within the uncertainties, the local structure (inter-atomic distances and Debye–Waller (DW) factors) of the bulk and films are very similar; DW factors for all samples and orientations generally increase with path length. EXAFS analysis found that the distances in the macrocycle within 3.5 Å from the central Zn exhibit very small variations. The macrocycle in the disordered TF has a slightly expanded structure and some cases have higher DW factors compared to both the bulk and the ordered TF.

XANES and multiple scattering analysis

We analyzed the Zn K-edge XANES by adopting a full multiple scattering approach in order to determine the structural differences in the studied films. Simulations of the Zn K-edge are performed using the MXAN code using a muffin tin potential.

In the shell-by-shell simulations (Fig. 7, right panel) the theoretical spectra were obtained by increasing the number of atoms in the single molecule structure (Fig. 1, conformer labeled d). The atoms included are drawn in the side panel. The experimental bulk sample spectrum is shown for comparison. The appearance of the structures obtained by increasing the number of atoms provides an indication of the scattering paths related to the spectral features.[48] The 5-atom calculation (*i.e.*, the macrocycle in the porphine structure) reproduces the main features, including the experimental peak at 9660 eV,

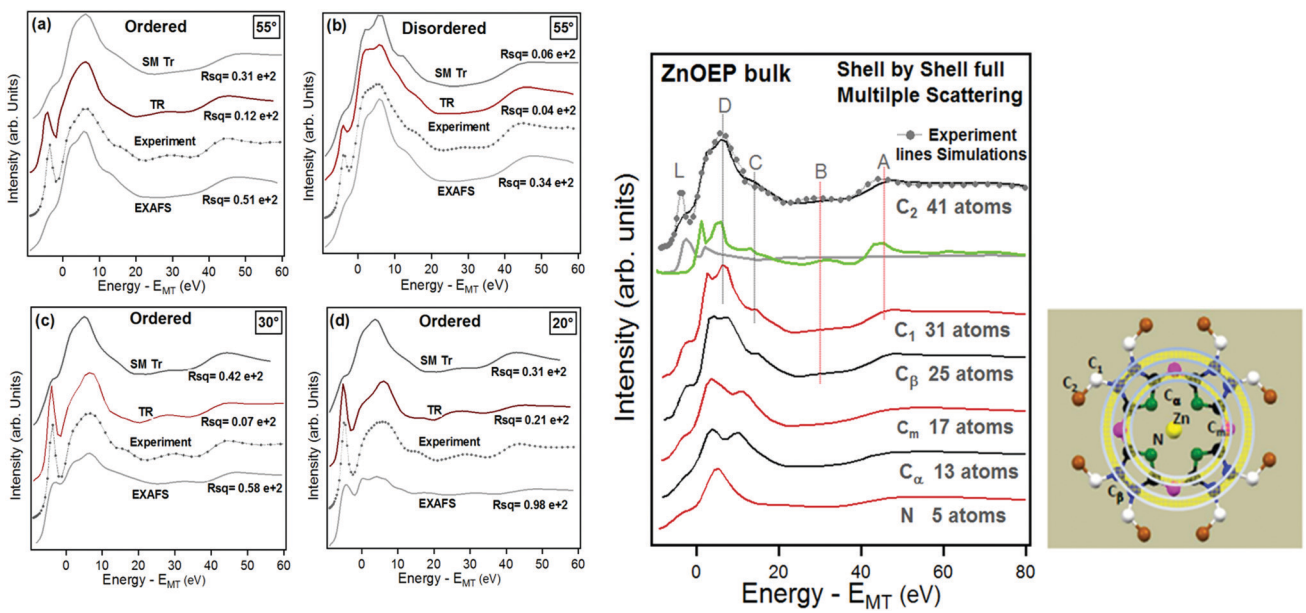

Fig. 7 (Left panel) Comparison of the Zn K edge spectra (dots) and the MXAN simulations for the disordered and ordered films taken at magic angle 55° (top panel) and (bottom panel) at 20° and 30°. Solid lines are the simulations obtained from the structure extracted from EXAFS analysis (gray lines) and best fits obtained by the optimization of the outer C atoms shells in the triclinic structure (TR) and in the single molecule (SM) structures. The residual square (R_{sq}) value for each simulation is also reported. (Right panel) MXAN simulations of the ZnOEP conformer molecule in the triclinic structure for θ = 55° (magic angle) compared to the Zn K edge XANES of the bulk sample. The labels indicate the most external atoms taken into account and refer to the figure of the conformer structure with the shells. The energy origin corresponds to the calculated muffin tin interstitial potential. For the 41 atoms case the in- (*x*, *y* green line) and out-of-plane (*z* gray line) calculated components are also shown. The shells of the ZnOEP molecule are shown in the right panel.

assigned to transitions to the LUMO, with the amplitude maximum along the direction perpendicular to the macrocycle plane (z), though the details are improved by increasing the simulation radius. MXAN analysis shows that the transitions at higher energy involve molecular orbitals which derive from the external carbon atoms. Further details of the fitting procedure are given in the ESI† (SI-6 sections).

Fig. 7 (left panel) shows the MXAN best fits for the Zn K edge spectra taken at magic angles of 55°, 30° and 20° for the ordered and disordered TFs. Zn K edge simulated spectra obtained using the parameters obtained from the EXAFS fits are also compared with experimental results (dotted lines). MXAN fitting has been performed by adopting two different coordinate models: the single molecule (SM Tr) of Fig. 1d, and the TR structural model involving the addition of the nearest C and N atoms (Fig. 1b) of the top and bottom ZnOEP molecules within the triclinic structure.

Good quality simulations for the ordered ZnOEP TFs are obtained for an angle of 55°, indicating that the outer C atoms (C_α and C_β) exhibit a deformed symmetry in the case of ordered TFs. This observation establishes a symmetry reduction of skeletal carbon atoms due to higher molecular order and increased π stacking of ZnOEP molecules for ordered TFs adopting a triclinic structure. As shown in Table 2, outer C atoms (C_α and C_β) do not present a deformed symmetry for disordered films in contrast to ordered ZnOEP TFs.

This observation highlights the implications of molecular order on electronic properties. While the average Zn–C_β distance remains practically unchanged, a weak reduction of the square symmetry (C_{4v}) of the C_β shell is found, with longer distances along the X direction (see the inset in Table 2) in the plane. The fit based on the TR structure is significantly better than that based on the SM model. Moreover, the intermolecular distances of the nearest molecules ($N_{up/down}$ and $C_{up/down}$ atoms) are less perturbed than in the disordered case. The fits performed at angles closer to the normal *i.e.* for scattering paths including molecules belonging to different planes of the triclinic structure exhibit a worst fit quality and an ambiguous solution of the structural simulations is obtained. Similar procedures and findings have been obtained for the semiordered spectra and reported in Table 2. In particular, for 20° and 30° spectra the simulations based on the EXAFS results were found to be in a very poor agreement.

Discussion

It is evident from Fig. 8(a) that an ordered stacking of molecules favours substantial π–π interactions. The calculated charge density contours determined from our simulations depict the influence of the π electron cloud on the neighbouring molecules in the triclinic ZnOEP framework as shown in Fig. 8(b). Small Raman shifts observed in the higher frequency range corresponding to skeletal carbon atoms (C_β, C_m, and C_α) for the ordered films compared to disordered films can be attributed to alterations of π charge density. It has been reported that molecular stacking induced alterations in the π charge density can lead to minor Raman shifts for the porphyrin TFs.[36]

The N K edge XANES spectra of the three differently ordered films are very similar, suggesting that structural variations of the macrocycle are very small. This result is complementary to the Raman spectroscopy observation in which no significant Raman shift has been observed for macrocycle vibrational modes.

The structural MXAN fits of the Zn K edge spectra reveal that spectral features for the disordered film can be reproduced considering 25 atoms instead of 31 atoms for ordered films, as indicated by the shell by shell analyses in Fig. SI-6 (ESI†). It suggests that, due to random molecular stacking, in disordered films the orientation of the ethyl groups (C_1 and C_2) with respect to C_β is not well defined. As shown in Fig. 3a, two peaks at 225 cm^{-1} and 245 cm^{-1} related to ethyl group vibrational modes are absent for disordered films, revealing the impact of ethyl groups' (C_1 and C_2) random orientations due to molecular disorder. This observation highlights the influence of molecular order on the electronic and vibrational properties of the molecular films.

Using XRD, Melamed *et al.* reported that 40 nm thick ZnOEP TFs on SiOx/Si have orientation along the (0 −1 1) direction perpendicular to the substrate, with ZnOEP molecules inclined by 50° with respect to the substrate.[41]

These observations are in good agreement with ours and agree with the observation that the XRD patterns of semiordered ZnOEP

Table 2 List of the ZnOEP distances in Å, as found by the structural MXAN fit by using the different models described in the text (see Fig. 1). The X and Y directions are described in the inlet. Confusion indicates a substantial insensitivity of the simulation to the ethyl C_1 and C_2 coordinates

	Model	EXAFS	Disordered SM Tr	Disordered TR	Semi-ordered SM Tr	Ordered SM Tr	Ordered TR
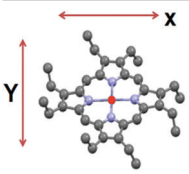	Best Fit R_{sq} parameter	—	0.06 e2	0.04 e2	0.4 e2	0.31 e2	0.12 e2
	Zn-C_β/Å	4.3	4.29 along X 4.31 along Y	4.29 along X 4.30 along Y	4.26 along X 4.34 along Y	4.29 along X 4.33 along Y	4.24 along X 4.36 along Y
	N_{up}–N_{down}/Å	3.59	—	3.48	3.51	—	3.55
	$C_\alpha up$–$C_z d$/Å	3.34	—	3.2	3.30	—	3.36
	Zn–C1/Å	5.63	Confusion ring 5.93 along X 5.53 along Y	Confusion ring 5.87 along X 5.55 along Y	5.93 along X 5.37 along Y	5.95 along X 5.32 along Y	5.84 along X 5.50 along Y
	Zn–C2/Å	6.33 along X 6.13 along Y	Confusion ring 6.58 along X 6.20 along Y	Confusion ring 6.57 along X 6.12 along Y	6.47 along X 6.00 along Y	6.47 along X 6.00 along Y	6.42 along X 6.03 along Y

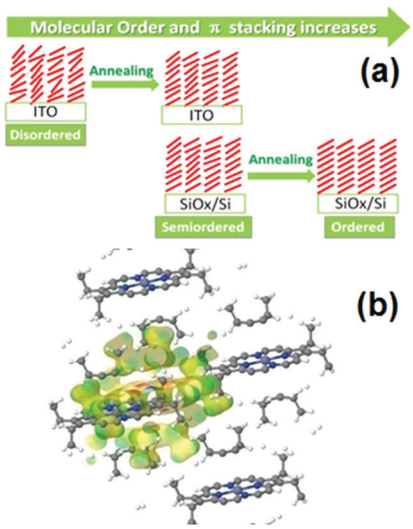

Fig. 8 (a) Schematic representation of the enhanced molecular order of ZnOEP molecules depending on the substrate and annealing. (b) Charge density contours as calculated in the triclinic ZnOEP structure between neighbour molecules.

films on the SiOx/Si substrate are similar to those deposited on ITO/glass. At variance with the semiordered film, we obtained an angle of about 45° for the ordered films with respect to the substrate. It appears that annealing of the ZnOEP TFs deposited on SiOx/Si at 80 °C improves the ordering with a small but notable change in the angle of orientation, as shown in Fig. 5(b).

In addition, our detailed MXAN fitting analysis of XANES spectra establishes a symmetry reduction in the molecular conformer involving C_β and C_α carbon atoms highlighting the consequences of increased π stacking of ZnOEP molecules adopting the triclinic structure. Such a strain in the structure is not observed in the macrocycle as shown in Table 2. These observations complement the Raman results which detected no Raman shift for the vibrational modes involving the macrocycle while, small but detectable Raman shifts were observed for the vibrational modes of skeletal carbon atoms for the ordered films as compared to semiordered and disordered films.

The probable cause of such asymmetrical stretching of the skeletal carbon atoms can be intermolecular interactions due to proximity with neighboring molecules in the triclinic framework. Such alterations of the π conjugation network are not expected for disordered films grown on ITO at room temperature. Thus, we anticipate higher cell efficiency for the ordered ZnOEP TFs on SiOx/Si obtained by annealing films grown at room temperature.

Conclusions

Summarizing, our work highlights the consequences of different degrees of long range order of ZnOEP TFs grown on SiOx/Si and ITO substrates with different roughnesses, with or without subsequent annealing. GIXRD analysis reveals that the TFs exhibit different degrees of long-range ordering, and average crystallites size, in good agreement with AFM. Although remarkable differences are found in the intramolecular reorganization, the effect of the disorder is mainly related to the skeletal carbon atoms' (C_α, C_β and C_1, C_2) outer shell displacements. Within the molecules, the macrocycle and the C atoms up to distances smaller than 4 Å remain almost unperturbed for ordered and disordered films. The local structure of nitrogen atoms is essentially unchanged, as also shown by N K edge NEXAFS.

This study provides useful insights for the optimization of the growth and control of the physical properties of functional molecular TFs, which are crucial for technological applications of organic semiconductors.

Conflicts of interest

There are no conflicts to declare.

Acknowledgements

S. C. and M. P. acknowledge the COST EuSpec. D. N. acknowledges CBM scrl for providing access to the BioNanoAnalysis core facility. This work is based on measurements taken after BACH ELETTRA 20130071 and 20140293 and GILDA ESRF 08-01 945 proposals. This project is partially supported by the Italian MIUR through the Progetto PIK EXPROREL and Eurofel. The CNR-IOM technical staff, Federico Salvador, Paolo Bertoch, Davide Benedetti and Andrea Martin, are kindly acknowledged for their support.

References

1 Y. Y. Noh, J. J. Kim, Y. Yoshida and K. Yase, *Adv. Mater.*, 2003, **15**, 699–702.
2 A. Suzuki, H. Ueda, Y. Okada, Y. Ohishi, Y. Yamasaki and T. Oku, *Chem. Mater. Eng.*, 2017, **5**, 34–42.
3 B. P. Rand, D. Cheyns and K. Vasseur, *Adv. Funct. Mater.*, 2012, **22**, 2987–2995.
4 A. Dey, A. Singh, D. Das and P. K. Iyer, *ACS Omega*, 2017, **2**, 1241–1248.
5 G. Run-Da, Y. Shou-Zhen, W. Peng, C. Yu, Z. Yi and L. Shi-Yong, *Chin. Phys. B*, 2013, **22**(12), 127304.
6 V. Coropceanu and J. Bredas, *Chem. Rev.*, 2007, **107**, 926–952.
7 S. Heutz, S. M. Bayliss, R. L. Middleton, G. Rumbles and T. S. Jones, *J. Phys. Chem. B*, 2000, **104**, 7124–7129.
8 M. M. El-Nahass, H. M. Zeyada, M. S. Aziz and N. A. El-GhamazOptical, *Materials*, 2004, **27**, 491–498.
9 S. Ryuzaki and J. Onoe, *J. Appl. Phys.*, 2008, **103**, 033516.
10 S. Ryuzaki, T. Kai, Y. Toda, S. Adachi and J. Onoe, *J. Phys. D: Appl. Phys.*, 2011, **44**, 145103.
11 R. Noriega, J. Rivnay, K. Vandewal, F. P. V. Koch, N. Stingelin, P. Smith, M. F. Toney and A. Salleo, *Nat. Mater.*, 2013, **12**, 1038–1044.
12 Y. Gao, *Mater. Sci. Eng., R*, 2010, **R68**, 39–87.

13 J. L. Brédas, J. P. Calbert, D. A. da Silva Filho and J. Cornil, *Proc. Natl. Acad. Sci. U. S. A.*, 2002, **99**, 5804–5809.

14 T. Minari, M. Seto, T. Nemoto, S. Isoda, K. Tsukagoshi and Y. Aoyagi, *Appl. Phys. Lett.*, 2007, **91**, 123501.

15 M. Campione, E. Fumagalli, L. Raimondo, A. Monguzzi, F. Meinardi and A. Sassella, *Chem. Mater.*, 2011, **23**, 832–840.

16 A. D. Phan, D. T. Nga, T.-L. Phan, L. T. M. Thanh, C. T. Anh, S. Bernad and N. A. Viet, *Phys. Rev. E: Stat., Nonlinear, Soft Matter Phys.*, 2014, **90**, 062707.

17 J.-H. Perng and D. F. Bocian, *J. Phys. Chem.*, 1992, **96**, 4804–4811.

18 L. Edwards, D. H. Dolphin and M. Gouterman, *J. Mol. Spectrosc.*, 1970, **36**, 90–109.

19 J. Onoe, S. Watanabe, S. Kato, M. Nakaya and J.-P. Bucher, *J. Chem. Phys.*, 2017, **147**, 214701.

Q7 20 H. J. Callot and R. Ocampo, *The Porphyrin Handbook*, *Academic Press*, *New York*, 2000, vol. 1.

21 A. Ozarowski, L. H. Man and A. L. Balch, *J. Am. Chem. Soc.*, 2003, **125**, 12606–12614.

22 M. Okazaki and C. A. McDowell, *J. Am. Chem. Soc.*, 1984, **106**, 3185–3190; L. Frydman, A. C. Olivieri, L. E. Diaz, A. Valasinas and B. Frydman, *J. Am. Chem. Soc.*, 1988, **110**, 5651–5661; H. X. Ji, J. S. Hu and L. J. Wan, *Chem. Commun.*, 2013, **23**, 2653–2655.

23 The term Near Edge X-ray Absorption Spectroscopy (NEXAFS) is mostly used in the soft X-ray spectral region while X-ray Absorption Near Edge Structure (XANES) is more common in the hard X-rays.

24 F. d'Acapito, A. Trapananti, S. Torrengo and S. Mobilio, *Neutron and Synchrotron Light news*, 2014, **19**, 2.

25 G. Ciatto, F. d'Acapito, F. Boscherini and S. Mobilio, *J. Synchrotron Radiat.*, 2004, **11**, 278.

26 M. Zangrando, M. Zacchigna, M. Finazzi, D. Cocco, R. Rochow and F. Parmigiani, *Rev. Sci. Instrum.*, 2004, **75**, 31–36.

27 G. Drera, G. Salvinelli, J. Åhlund, P. G. Karlsson, B. Wannberg, E. Magnano, S. Nappini and L. Sangaletti, *J. Electron Spectrosc. Relat. Phenom.*, 2014, **195**, 109–116.

28 M. Benfatto and S. D. Longa, *J. Synchrotron Radiat.*, 2018, 1087–1094.

29 M. Benfatto and S. D. Longa, *J. Phys.: Conf. Ser.*, 2009, **190**, 12031.

30 A. Lausi, M. Polentarutti, S. Onesti, J. R. Plaisier, E. Busetto, G. Bais, L. Barba, A. Cassetta, G. Campi and D. Lamba, *et al.*, *Eur. Phys. J. Plus*, 2015, **130**, 1–8.

31 G. Scavia, L. Barba, G. Arrighetti, S. Milita and W. Porzio, *Eur. Polym. J.*, 2012, **48**, 1050–1061.

32 www.ccdc.cam.ac.uk.

33 D. W. Breiby, O. Bunk, J. W. Andreasen, H. T. Lemke and M. M. Nielsen, Simulating X-ray diffraction of textured films, *J. Appl. Crystallogr.*, 2008, **41**, 262–271.

34 T. Roisnel and J. R. Carvajal, *Mater. Sci. Forum*, 2001, **378**, 118.

35 A. M. Hindeleh and R. Hosemann, *J. Mater. Sci.*, 1991, **26**, 5127–5133; R. Hosemann and A. M. Hindeleh, *J. Macromol. Sci. Phys. B*, 1995, **35**, 327–336.

36 J. R. Ares, A. Pascual, I. J. Ferrer and C. Sánchez, *Thin Solid Films*, 2005, **480**, 477.

37 A. Kumar, D. Naumenko, L. Cozzarini, L. Barba, A. Cassetta and M. Pedio, *J. Raman Spectrosc.*, 2018, 1–8.

38 J.-H. Perng and D. F. Bocian, *J. Phys. Chem.*, 1992, **96**(12), 4804–4811.

39 M. Abe, T. Kitagawa and Y. Kyogoku, *J. Phys. Chem.*, 1978, **69**, 4526.

40 L. D. Sparks, W. R. Scheidt and J. A. Shelnutt, *J. Am. Chem. Soc.*, 1988, **110**, 12.

41 D. Melamed, B. Darlington, D. J. R. Brook, H. L. Pan, A. Campion and M. A. Fox, *J. Phys. Chem.*, 1994, **98**, 8971–8976.

42 N. Coppede, T. Toccoli, A. Pallaoro, F. Siviero, K. Walzer, M. Castriota, E. Cazzanelli and S. Iannotta, *J. Phys. Chem. A*, 2007, **111**, 12550–12558.

43 C. S. Guo, L. Sun, K. Hermann, C. F. Hermanns, M. Bernien and W. Kuch, *J. Chem. Phys.*, 2012, **137**, 194703.

44 G. Rossi, F. d'Acapito, L. Amidani, F. Boscherini and M. Pedio, *Phys. Chem. Chem. Phys.*, 2016, **18**, 23686–23694.

45 S. Ryuzaki, T. Hasegawa and J. Onoe, *J. Appl. Phys.*, 2009, **105**, 113529.

46 In the case of aged samples C1s broadening and oxygen contamination in the O1s data have been observed due to adsorbed oxygen and water vapour from the atmosphere. In contrast, short term air exposed samples do not show this trend.

47 S. Pascarelli, F. Boscherini, F. D'Acapito, J. Hrdy, C. Meneghini and S. Mobilio, *J. Synchrotron Radiat.*, 1996, **3**, 147.

48 I. M. Alecu, J. Zheng, Y. Zhao and D. G. Truhlar, *J. Chem. Theory Comput.*, 2010, **6**, 2872.